

Calculation of Mutual Inductance between Circular and Arbitrarily Shaped Filaments via Segmentation Method

Kirill V. Poletkin, Slobodan Babic, Sreejith Sasi Kumar and Emil R. Mamleyev

Abstract—In this article, two analytical formulas for the calculation of mutual inductance between a circular filament and line segment arbitrarily positioning in the space are derived by using Mutual Inductance Method (MIM) and Babic's Method (BM), respectively. Using the fact that any curve can be interpolated by a set of line segments, a method for calculation of mutual inductance between a circular filament and filament having an arbitrary shape in the space is proposed based on the derived analytical formulas. The derived two formulas and the proposed method (Segmentation Method) were numerically validated by using FastHenry software and reference examples from the literature. In particular, the proposed method was successfully applied to the calculation of mutual inductance between the circular filament and the following special curves such as circle, circular arc, elliptic arc, ellipse, spiral, helices and conical helices. All results of the calculation are in good agreement with the reference examples.

Index Terms—mutual inductance, analytical formula, circular filament, special functions, complete elliptic functions, segment.

I. INTRODUCTION

ANALYTICAL and semi-analytical methods in the calculation of self- and mutual-inductances of conducting elements of electrical circuits have played an important role in development of power transfer, wireless communication, sensing and actuation and have been applied in a broad fields of science, including electrical and electronic engineering, medicine, physics, nuclear magnetic resonance, mechatronics and robotics, to designate the most prominent.

Although, a number of efficient numerical methods implemented in the commercially developed software are available, analytical and semi-analytical methods allow to obtaining the result of calculations in the form of a final formula with a finite number of input parameters, which when applicable may significantly reduce computation effort. Providing the direct access to a calculational formula for a user in such methods facilitates mathematical analysis of obtained results of calculation and opens an opportunity for their further optimization.

In particular, calculation of mutual inductance between a circular filament and systems of filaments of different shapes

is a prime example of application of such analytical methods. Albeit, collections of formulas for the calculation of mutual inductance between filaments of different geometrical shapes covering a wide spectrum of practical arrangements have variously been presented in classical handbooks by Rosa [1], Grover [2], Dwight [3], Snow [4], Zeitlin [5], Kalantarov [6], among others. However, these analytical methods have proved their efficiency and have been successfully employed in an increasing number of applications, including electromagnetic levitation [7], [8], superconducting levitation [9], calculation of mutual inductance between thick coils [10]–[15], magnetic force and torque calculation between circular coils [16]–[20], calculation of magnetic stiffness [21], [22], wireless power transfer [23]–[25], electromagnetic actuation [26]–[28], micro-machined contactless inductive suspensions [29]–[31] and hybrid contactless suspensions [32]–[35], biomedical applications [36], [37], topology optimization of coils [38], nuclear magnetic resonance [39], [40], indoor positioning systems [41], navigation sensors [42], wireless power transfer systems [43], [44], magneto-inductive wireless communications [45] and others.

Kalantarov and Zeitlin showed that the calculation of mutual inductance between a circular primary filament and any other secondary filament having an arbitrary shape and any desired position with respect to the primary filament can be reduced to a line integral [6, Sec. 1-12, page 49]. Adapting this result, Poletkin derived the analytical formulas for calculating the mutual inductance between two circular filaments having any desired position with respect to each other in work [12], as an alternative to Grover's and Babic's expressions reported in works [2] and [11], respectively.

Moreover, it was mentioned in work [12] that the obtained formula for the treatment of the singular case, when the circular filaments are mutually perpendicular, can be applied also to the calculation of the mutual inductance between a circle and line segment after taking a minor modification of the original formula. Using this fact and an alternative approach developed by Babic [11], two analytical formulas for calculation of mutual inductance between a circular filament and line segment arbitrarily positioning in the space are derived by means of MIM and BM, respectively.

Since, any curve can be interpolated with a desired accuracy by a finite number of line segments, a segmentation method for calculation of the mutual inductance between the primary circle and a filament having an arbitrary shape is proposed and successfully developed based on the two derived formulas

E. R. Mamleyev and K. V. Poletkin are with Institute of Microstructure Technology, Karlsruhe Institute of Technology, Hermann-von-Helmholtz-Platz 1, 76344 Eggenstein-Leopoldshafen, Germany.

K. V. Poletkin is also with New Uzbekistan University, Mustaqillik ave. 54, 100007 Tashkent, Uzbekistan e-mail: k.poletkin@newuu.uz.

S. Babic is an independent researcher; 53 Berlioz 101, H3E 1N2, Montréal, Québec, Canada e-mail: slobobob@yahoo.com.

S. S. Kumar is with Technische Universität Ilmenau, Ehrenbergstraße 29, 98693 Ilmenau, Germany.

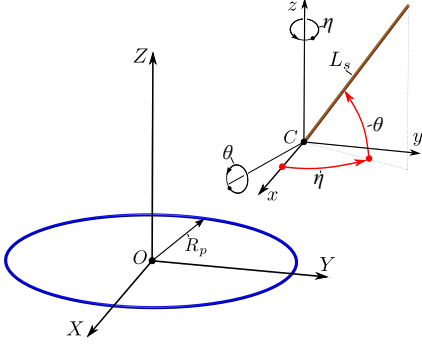


Fig. 1. General scheme of arbitrarily positioning the line segment with respect to the circular filament: R_p is the radius of the circle and L_s is the length of the line segment.

for calculation of the mutual inductance between the circle and line segment. It is shown that for calculation of mutual inductance by means of the segmentation method, a set of points belonging to the arbitrarily shaped filament as the input data is only needed. The developed methodology is successfully applied to the calculation of mutual inductance between the circular filament and the following special curves such as circle, circular arc, elliptic arc, ellipse, spiral, helices and conical helices. All results of calculation are in a good agreement with the reference examples and successfully validated by the *FastHenry* software [46].

II. MUTUAL INDUCTANCE BETWEEN CIRCULAR FILAMENT AND LINE SEGMENT

Let us consider the filament system consisting of a primary circular filament having a radius of R_p and a secondary filament represented as a line segment having a length of L_s , which is arbitrarily positioned in the space with respect to the primary circle as shown in Fig. 1. A coordinate frame (CF) denoted as XYZ is assigned to the primary circle in a such way that the Z axis is coincident with the circle axis and the XOY plane of the CF lies on circle's plane, where the origin O corresponds to the centre of primary circle. In turn, the xyz CF is assigned to the secondary filament so that its origin C is attached to one of its endpoints. The axes of the xyz CF are parallel to the axes of XYZ , respectively.

The linear position of the secondary filament with respect to the primary one is defined by the coordinates of the origin C (x_C, y_C, z_C). The angular position of the line segment is defined by the angle η and θ corresponding to the angular rotation around the z -axis of the plane passing through the z -axis and line segment, and then the rotation of the segment around an axis, which is perpendicular to this segment- z plane and passing through the origin C , respectively, as shown in Fig. 1.

A. Mutual Inductance Method (MIM)

The mutual inductance between the circular filament and the line segment arbitrarily orientated in the space can be calculated by the following formula, which is derived by

using Kalantarov-Zeitlin's approach reported in work [12]. Introducing the following dimensionless coordinates:

$$x = \frac{x_C}{L_s}, \quad y = \frac{y_C}{L_s}, \quad z = \frac{z_C}{L_s}, \quad s = \sqrt{x^2 + y^2}, \quad (1)$$

the formula can be written as

$$M = \frac{\mu_0 \sqrt{R_p L_s}}{\pi} \int_0^1 U \cdot \Phi(k) d\bar{\ell}, \quad (2)$$

where μ_0 is the magnetic permeability of free space, $\bar{\ell} = \ell/L_s$ is the dimensionless integrating variable,

$$U = U(x, y, \eta, \theta) = \frac{t_1 - t_2}{\rho^{1.5}} \cdot \cos \theta, \quad (3)$$

$$\begin{aligned} t_1 &= t_1(x, \eta, \theta) = \sin \eta \cdot (x + \bar{\ell} \cos \theta \cos \eta), \\ t_2 &= t_2(y, \eta, \theta) = \cos \eta \cdot (y + \bar{\ell} \cos \theta \sin \eta), \\ \rho &= \rho(x, y, \eta, \theta) = \sqrt{s^2 + 2\bar{\ell} \cos \theta \cdot (x \cos(\eta) + y \sin(\eta)) + \bar{\ell}^2 \cos^2 \theta}, \end{aligned} \quad (4)$$

$$\Phi(k) = \frac{1}{k} \left[\left(1 - \frac{k^2}{2} \right) K(k) - E(k) \right], \quad (5)$$

and $K(k)$ and $E(k)$ are the complete elliptic functions of the first and second kind, respectively, and

$$\begin{aligned} k^2 &= k^2(x, y, z, \theta, \eta) = \frac{4\nu\rho}{(\nu\rho + 1)^2 + \nu^2 z_\lambda^2}, \\ \nu &= L_s/R_p, \quad z_\lambda = z + \bar{\ell} \sin \theta. \end{aligned} \quad (6)$$

B. Babic's Method (BM)

Let us consider again the calculation scheme shown in Fig. 1, but in a difference with MIM the line segment is given by coordinates of its two endpoints, namely, $p_0(x_0, y_0, z_0)$ and $p_1(x_1, y_1, z_1)$.

Then, the coordinates of an arbitrary point S (x_s, y_s, z_s) of the secondary line segment can be written parametrically as follows:

$$x_s = q\bar{\ell} + x_0, \quad y_s = r\bar{\ell} + y_0, \quad z_s = s\bar{\ell} + z_0, \quad \bar{\ell} \in [0, 1], \quad (7)$$

where $q = x_1 - x_0$, $r = y_1 - y_0$, $s = z_1 - z_0$. Hence, the differential element of the line segment becomes

$$d\vec{l}_s = \{q, r, s\} d\bar{\ell}, \quad \bar{\ell} \in [0, 1]. \quad (8)$$

While, parametric coordinates of an arbitrary point P (x_p, y_p, z_p) of the primary circular filament can be defined by the following expressions:

$$x_p = R_p \cos \phi, \quad y_p = R_p \sin \phi, \quad z_p = 0, \quad \phi \in [0, 2\pi]. \quad (9)$$

The differential of the primary circular filament is given by

$$d\vec{l}_p = R_p \{-\sin \phi, \cos \phi, 0\} d\phi, \quad \phi \in [0, 2\pi]. \quad (10)$$

Accounting for equations (10) and (8), the mutual inductance between circular filament and the line segment can be calculated by

$$\begin{aligned} M &= \frac{\mu_0}{4\pi} \int_0^1 \int_0^{2\pi} \frac{d\vec{l}_p \cdot d\vec{l}_s}{r_{ps}} = \\ &= \frac{\mu_0 R_p}{4\pi} \int_0^1 \int_0^{2\pi} \frac{-q \sin \phi + r \cos \phi}{r_{ps}} d\phi d\bar{\ell}, \end{aligned} \quad (11)$$

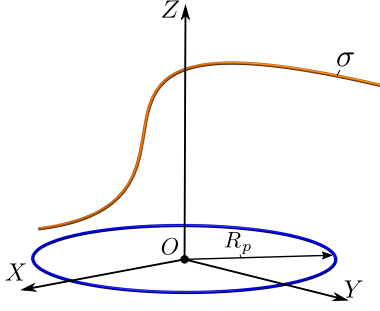


Fig. 2. General scheme of arbitrary shaped filament and the circular filament.

where

$$r_{ps}^2 = (x_s - R_p \cos(\phi))^2 + (y_s - R_p \sin(\phi))^2 + z_s^2. \quad (12)$$

The following integral

$$I = \int_0^{2\pi} \frac{-q \sin \phi + r \cos \phi}{r_{ps}} d\phi \quad (13)$$

can be expressed via the complete elliptic functions of the first and second kind $K(k)$ and $E(k)$, respectively, as follows

$$I = \frac{2V}{\sqrt{R_p} \sqrt{p^3}} \Psi(k), \quad (14)$$

where

$$\begin{aligned} V &= r \cdot x_s - q \cdot y_s, \quad p = \sqrt{x_s^2 + y_s^2}, \\ \Psi(k) &= \left(\frac{2}{k} - k \right) K(k) - \frac{2}{k} E(k), \\ k^2 &= \frac{4R_p p}{(R_p + p)^2 + z_s^2}. \end{aligned} \quad (15)$$

Hence, replacing the integral (13) in (11) by (14), the final formula for calculation of mutual inductance becomes

$$M = \frac{\mu_0 \sqrt{R_p}}{2\pi} \int_0^1 \frac{V}{\sqrt{p^3}} \Psi(k) d\bar{\ell}. \quad (16)$$

The input parameters for Babic's and MI method are related by the following relationships:

$$\begin{aligned} L_s^2 &= q^2 + r^2 + s^2, \\ \eta &= \tan^{-1} \left(\frac{r}{q} \right), \quad \theta = \tan^{-1} \left(\frac{s}{\sqrt{q^2 + r^2}} \right). \end{aligned} \quad (17)$$

Worth noting that according to (2) and (16) the mutual inductance is equal to zero, when the line segment crosses the Z axis or is located on a line crossing the Z axis.

III. SEGMENTATION METHOD

The secondary filament having an arbitrary shape and the primary circular filament of a radius R_p are considered as shown in Fig. 2. The secondary filament is given, for instance, by a 3D parametric curve $\sigma = \sigma(\ell)$, where ℓ is the parameter defined within a finite interval $[\varphi_0, \varphi_1]$, and the following inequality $\varphi_1 > \varphi_0 \geq 0$ is valid.

It is assumed that the curve is sampled by n points, so that we have $\underline{p}_0(h_0)$, $\underline{p}_1(h_1)$, $\underline{p}_2(h_2)$, \dots , $\underline{p}_{n-1}(h_{n-1})$, $\underline{p}_n(h_n)$. The points can be defined in the following way

$$\underline{p}_i(h_i) = [x_\sigma(h_i) \ y_\sigma(h_i) \ z_\sigma(h_i)]^T, \quad i = 0 \dots n, \quad (18)$$

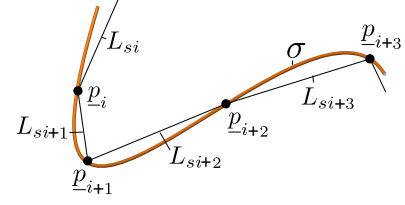


Fig. 3. Interpolation of the σ curve by line segments.

as (3×1) -column-matrices, where x_σ , y_σ and z_σ are the coordinates of the σ -curve and

$$h_i = h_{i-1} + (\varphi_1 - \varphi_0)/n, \quad i = 1 \dots n, \quad (19)$$

and so $h_0 = \varphi_0$. Using the set of points (18) and (19), the σ -curve can be interpolated by line segments as shown in Fig. 3. The length of each line segment can be calculated by

$$L_{si}^2 = (\underline{p}_i - \underline{p}_{i-1})^T (\underline{p}_i - \underline{p}_{i-1}), \quad (20)$$

while the angles and dimensionless coordinates of i -th line segment become

$$\begin{aligned} \eta_i &= \tan^{-1} \left(\frac{\underline{p}_{yi} - \underline{p}_{yi-1}}{\underline{p}_{xi} - \underline{p}_{xi-1}} \right), \\ \theta_i &= \tan^{-1} \left(\frac{\underline{p}_{zi} - \underline{p}_{zi-1}}{\sqrt{(\underline{p}_{xi} - \underline{p}_{xi-1})^2 + (\underline{p}_{yi} - \underline{p}_{yi-1})^2}} \right); \end{aligned} \quad (21)$$

and

$$x_i = \frac{\underline{p}_{xi-1}}{L_{si}}, \quad y_i = \frac{\underline{p}_{yi-1}}{L_{si}}, \quad z_i = \frac{\underline{p}_{zi-1}}{L_{si}}, \quad s_i = \sqrt{x_i^2 + y_i^2}, \quad (22)$$

respectively. Substituting (20), (21) and (22) into (2), the mutual inductance M_i between the circular filament and i -th line segment can be calculated. Hence, performing summation of all n terms of M_i , the formula for calculation of the mutual inductance between the arbitrary shape and the primary circular filament can be written as follows

$$M_\sigma = \frac{\mu_0 \sqrt{R_p}}{\pi} \int_0^1 \sum_{i=1}^n \sqrt{L_{si}} \cdot U_i \cdot \Phi(k_i) d\bar{\ell}. \quad (23)$$

Alternatively, the calculation can be performed by using Babic's formula (16), namely,

$$M_\sigma = \frac{\mu_0 \sqrt{R_p}}{2\pi} \int_0^1 \sum_{i=1}^n \frac{V_i}{\sqrt{p_i^3}} \Psi(k_i) d\bar{\ell}. \quad (24)$$

Thus, interpolating the parametric σ -curve by n line segments, the calculation of the mutual inductance between the arbitrary shape and the primary circular filament can be performed by means of using developed formulas, namely, (2) and (16), which are applied n times to each interpolating line segment followed by summation executed by (23) and (24) for all obtained calculation results. The *Matlab* files with the implemented formulas (2), (16), (23) and (24) are available from the authors as supplementary materials to this article.

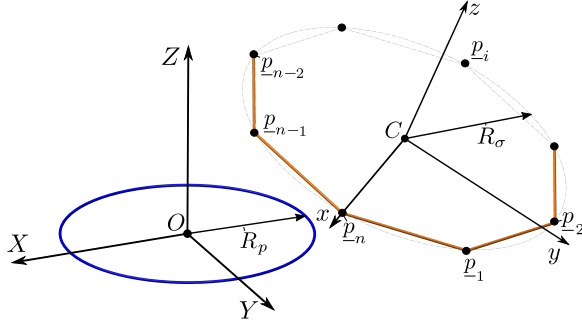


Fig. 4. A regular polygon of n sides arbitrarily positioned in the space with respect to the circle of radius R_p .

IV. EXAMPLES OF CALCULATION. NUMERICAL VERIFICATION

In this section the developed formulas (2) and (16), as well as the proposed segmentation method based on (23) and (24) are validated by using FastHenry software and reference examples from the literature.

A. Mutual inductance of line segment and circle

Example 1 : Let us suppose that the radius of primary circle is $R_p=1$ m and the line segment defined by two endpoints having the following coordinates, namely, $p_0(1 \text{ m}, 2 \text{ m}, 3 \text{ m})$ and $p_1(2 \text{ m}, 3 \text{ m}, 4 \text{ m})$. The results of calculation are

	FastHenry	BM, (16)	MIM, (2)
M, nH	-3.53653	-3.401894	-3.401894

Example 2 : Let us suppose that the radius of primary circle is $R_p=1$ m and the line segment defined by two endpoints having the following coordinates, namely, $p_0(1 \text{ m}, 1 \text{ m}, 1 \text{ m})$ and $p_1(0 \text{ m}, 1 \text{ m}, 1 \text{ m})$. The segment is parallel to the plane of the circle. The results of calculation are

	FastHenry	BM, (16)	MIM, (2)
M, nH	69.4492	69.51806	69.51806

Example 3 : Let us suppose that the radius of primary circle is $R_p=0.03$ m and the line segment defined by two endpoints having the following coordinates, namely, $p_0(0.0175 \text{ m}, -0.0029904 \text{ m}, 0.0040192 \text{ m})$ and $p_1(0.0025 \text{ m}, 0.02299 \text{ m}, 0.055981 \text{ m})$. The results of calculation are

	FastHenry	BM, (16)	MIM, (2)
M, nH	1.82457	1.83574	1.83574

B. Mutual inductance between circle and a regular polygon of n sides arbitrarily positioned in the space

In this section, the mutual inductance between a regular polygon of n sides, which is arbitrarily positioned in the space with respect to the circle of radius R_p is calculated by

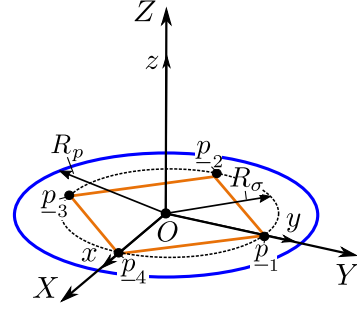


Fig. 5. Scheme for Example 4.

segmentation method based on (23) and (24). It is assumed that the polygon is inscribed in a circle of a radius R_σ lying on the xy plane as shown in Fig. 4. The parameter ℓ is defined within the finite interval $[0, 2\pi]$. This interval determines the distribution of the polygon vertices on the xy plane. In particular, n -th vertex within such interval of the parameter ℓ is located on the x axis. The linear misalignment of the polygon is defined by coordinates of point C corresponding to the centre of the secondary circle, while the angular misalignment can be defined by Grover's angles denoted by θ and η [12].

Then, input points can be calculated by

$$\underline{p}_i(h_i) = \begin{bmatrix} x_C \\ y_C \\ z_C \end{bmatrix} + \underline{\Lambda}_\theta^T \underline{\Lambda}_\eta^T \begin{bmatrix} R_\sigma \cos h_i \\ R_\sigma \sin h_i \\ 0 \end{bmatrix}, \quad i = 0 \dots n, \quad (25)$$

where

$$\underline{\Lambda}_\eta = \begin{bmatrix} \cos \eta & \sin \eta & 0 \\ -\sin \eta & \cos \eta & 0 \\ 0 & 0 & 1 \end{bmatrix}, \quad \underline{\Lambda}_\theta = \begin{bmatrix} 1 & 0 & 0 \\ 0 & \cos \theta & \sin \theta \\ 0 & -\sin \theta & \cos \theta \end{bmatrix}. \quad (26)$$

Example 4 (Example 1-3, page 50 in Kalantarov's book [6]): The primary circle of radius $R_p=1$ m and the square filament of a side length of 1 m (the polygon of $n = 4$ sides, $R_\sigma = \sqrt{2}/2 \approx 0.707$ m) are considered. The square is lying on the XY plane and its origin coincides with point O as shown in Fig. 5. The results of calculation show

	Kalantarov's book	FastHenry	BM, (24)	MIM, (23)
$M_\sigma, \mu\text{H}$	0.880	0.72949	0.73075	0.73075

Example 5 : Considering the same arrangement as in Example 4, but the centre of square filament is located at point C having the following coordinates $x_C = y_C = 0$ m and $z_C = 1 \text{ m}/\sqrt{2}$. The results of calculation are

	FastHenry	BM, (24)	MIM, (23)
$M_\sigma, \mu\text{H}$	0.317264	0.31754544	0.31754544

Example 6 : The primary circle has a radius of $R_p = 16$ cm. The triangular filament is inscribed in a circle having a radius of $R_\sigma = 10$ cm. The centre of the secondary circle has the following coordinates: $x_C = 0$, $y_C = 4.3301$ cm, and

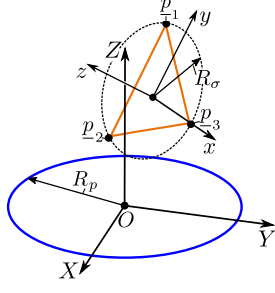


Fig. 6. Scheme for Example 6.

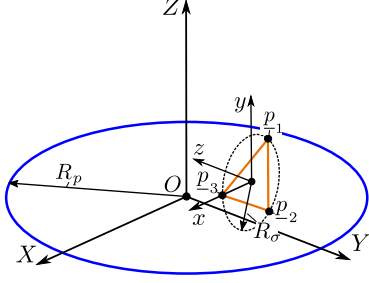


Fig. 7. Scheme for Example 9.

$z_C = 17.5$ cm. While, the angular misalignment is defined by the following Grover's angles, namely, $\eta = 45^\circ$ and $\theta = 60.0^\circ$ as shown in Fig. 6. The results of calculation are

	FastHenry	BM, (24)	MIM, (23)
M_{σ}, nH	5.94445	5.927887	5.927887

Example 7 : Using the same arrangement as in previous Example 6, the square polygon is inscribed. The results of calculation are

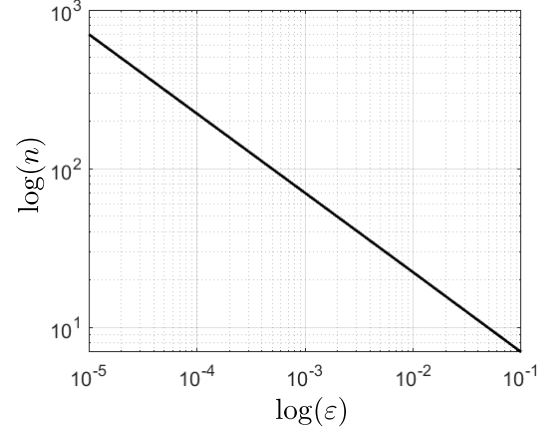
	FastHenry	BM, (24)	MIM, (23)
M_{σ}, nH	9.40649	9.435092	9.435092

Example 8 : The hexagon ($n = 6$ sides) is inscribed in the secondary circle of the same arrangement as in Example 6. The results of calculation are

	FastHenry	BM, (24)	MIM, (23)
M_{σ}, nH	12.4966	12.54164	12.54164

Example 9 : The primary circle has a radius of $R_p = 40$ cm. The triangular filament is inscribed in a circle having a radius of $R_{\sigma} = 10$ cm, which is perpendicular to the primary circle that Grover's angles of $\eta = 0^\circ$ and $\theta = 90.0^\circ$. The centre of the secondary circle has the following coordinates: $x_C = 0$, $y_C = 20$ cm, and $z_C = 10$ cm as shown Fig. 7. The results of calculation become

	FastHenry	BM, (24)	MIM, (23)
M_{σ}, nH	-4.65652	-4.686079	-4.686079

Fig. 8. The required number of line segments for given relative error of interpolation of a circle, $n = n(\epsilon)$.

Example 10 : Using the same arrangement as in Example 9, the square polygon is inscribed. The results of calculation are

	FastHenry	BM, (24)	MIM, (23)
M_{σ}, nH	-7.07775	-7.094651	-7.094651

Example 11 : Using the same arrangement as in Example 9, the hexagon is inscribed. The results of calculation are

	FastHenry	BM, (24)	MIM, (23)
M_{σ}, nH	-9.0490	-9.0334	-9.0334

C. Mutual inductance between two circular filaments

In this section, the method of segmentation is applied to the calculation of mutual inductance between two circular filaments arbitrarily orientated in the space with respect to each other. Similar to Sec.IV-B, the secondary circle is lying on the xy plane. The linear misalignment is defined by coordinates of point C corresponding to the centre of the secondary circle, and the angular misalignment is defined by Grover's angles denoted by θ and η [12]. The results of the calculation are compared with results obtained by means of analytical formulas developed by Babic in work [11] and Poletkin in [12].

The accuracy of interpolation of a circle by line segments can be measured by the relative error ϵ , which can be estimated as the difference between the radius of the circle and a length of a line joining a centre of the circle and mid point of a line segment divided by the radius:

$$\epsilon = 1 - \cos \frac{\pi}{n}. \quad (27)$$

Form (27) follows the obvious conclusion that the larger the number of line segments the smaller the error. The required number of line segments for the given relative error can be also evaluated by (27) and presented, for instance, in the logarithmic scale as shown in Fig. 8. As seen from Fig. 8,

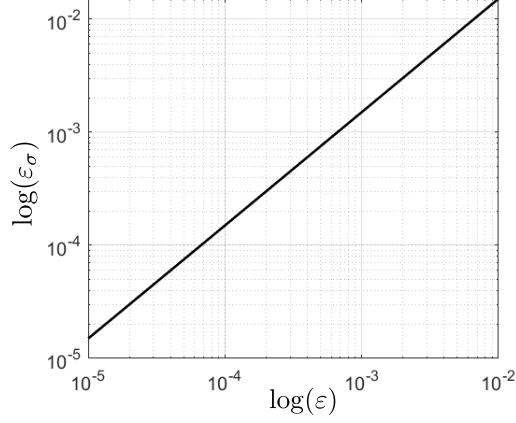


Fig. 9. The relative error of calculation of mutual inductance versus the relative error of interpolation of a circle by line segments.

to interpolate a circle with the relative error, for instance, less than 10^{-3} , the number of line segments must be more than 100.

For generating input points, equation (25) can be used with the only difference that the number of line segments is being chosen in according to the desired accuracy of interpolation of a circle, which in turn effects on the accuracy of calculation of mutual inductance.

Indeed, the accuracy of calculation of mutual inductance can be measured also by the relative error, which is defined as follows

$$\varepsilon_\sigma = \frac{M - M_\sigma}{M}, \quad (28)$$

where M is the mutual inductance calculated by Babic's or Poletkin's formula as mentioned above. Clearly that it is dependent on the number of line segments. To exam this point let us consider the following geometrical arrangement taken from Babic's work [11, page 3597, Example 12], as an illustrative example, in which two circles with radii $R_p = 16.0$ cm and $R_\sigma = 10.0$ cm and the centre of the secondary σ -circle is located at $x_C = 0$, $y_C = 4.3301$ cm, $z_C = 17.5$ cm and the angle, θ of 60.0° , but the η angle is chosen to be 45.0° as shown in Fig. 10. Performing calculation for different numbers

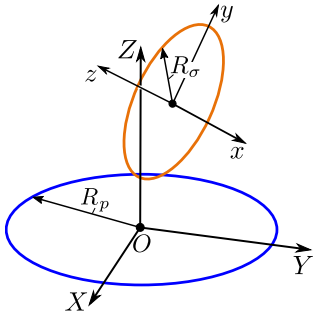


Fig. 10. Arrangement of circles in the illustrative example.

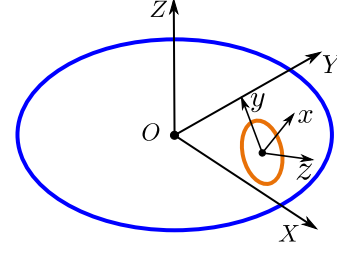


Fig. 11. Scheme for Example 12.

of line segments, the results are tabulated as follows

n	ε_σ	BM, (24), nH	MIM, (23), nH
22	0.015173	15.25271	15.25271
70	0.001507	15.46438	15.46438
222	0.000150	15.48539	15.48539
702	0.000015	15.48748	15.48748

Using the obtained results shown in the above table, the relative error ε_σ as a function of the number n of line segments can be defined, namely, $\varepsilon_\sigma = \varepsilon_\sigma(n)$. Moreover, both functions $\varepsilon_\sigma = \varepsilon_\sigma(n)$ and $n = n(\varepsilon)$ can be joined into one function exhibiting the dependency of the relative error of calculation mutual inductance on the relative error of interpolation of a circle as shown in Fig. 9. Although, Fig. 9 shows the evaluation of the error for the particular arrangement. However, the result is surprisingly consistence and can be used for the preliminary estimation of the error of calculation in other arrangements as shown below. For further calculation, the number of line segments is set to 200 that, according to Fig. 9, the error, ε_σ , is estimated to be around 0.00015.

Example 12: The primary and secondary circles have radii of $R_p = 5$ mm and $R_s = 1$ mm, respectively. The centre of the secondary circle is located at $x_C = 3$ mm, $y_C = 1$ mm, $z_C = 0.5$ mm and its angular misalignment are defined by $\theta = 57.6885^\circ$ and $\eta = 108.4349^\circ$ as shown in Fig. 11. The result of calculation is

n	ε_σ	BM, (24), nH	MIM, (23), nH
200	0.0001566	0.3577388	0.3577388

Example 13: The primary and secondary circles have radii $R_p = 40$ cm and $R_s = 5$ cm, respectively. The centre of the secondary circle is located at $x_C = 10$ cm, $y_C = 15$ cm, $z_C = 0.0$ cm. The angular misalignment of the secondary filament is defined as follows $\theta = 74.4986^\circ$ and $\eta = 123.6901^\circ$. As it has mentioned above, for calculation the number of line segments of $n = 200$ is taken. The result of calculation is

n	ε_σ	BM, (24), nH	MIM, (23), nH
200	0.0001615	3.848737	3.848737

Example 14 (Example 11, page 3596 in the Babič article [11]): Let us consider two circular filaments having radii of

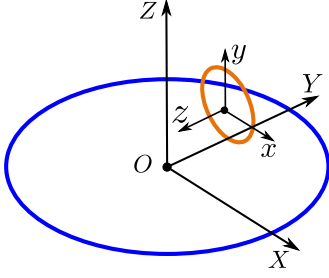


Fig. 12. Scheme for Example 14.

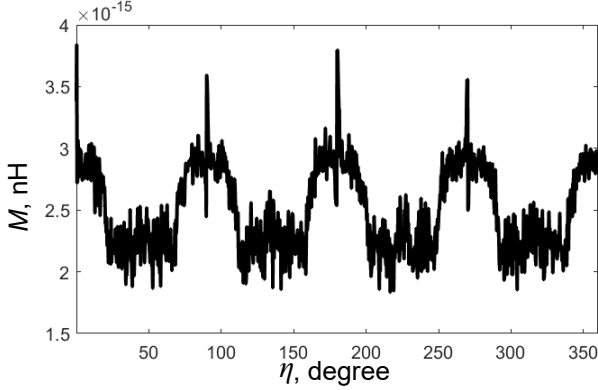


Fig. 13. The chaotic distribution of the absolute error against the η angle in Example 15.

$R_p = 40$ cm and $R_s = 10$ cm, which are mutually perpendicular to each other that angles of $\eta = 0$ and $\theta = 90.0^\circ$. The centre of the secondary circle has the following coordinates: $x_C = 0$, $y_C = 20$ cm, and $z_C = 10$ cm as shown in Fig. 12. The result becomes

n	ε_σ	BM, (24), nH	MIM, (23), nH
200	0.0001467	-10.72715	-10.72715

Example 15 (Example 21, Poletkin's article [12]): Mutually perpendicular circles (angles of $\theta = 90.0^\circ$ and $\eta = 0$) having the same radii as in Example 14 are considered, but the centre of the secondary coil is located at the origin O . Results of calculation are

n	BM, (24), nH	MIM, (23), nH
200	3.27233×10^{-15}	2.91992×10^{-15}

The results show the small error, which has the chaotic nature. Indeed, changing the angle η in a range of $0 < \eta \leq 360^\circ$ the chaotic distribution of the error is observed as shown in Fig. 13. Analysis of the figure depicts that the error does not exceed of 4×10^{-15} nH. Worth noting that varying the number of line segments, n , alters the error distribution, but keeps its value below the observed maximum.

Example 16 (Example 22, Poletkin's article [12]): Now we again consider mutually perpendicular circles having the same radii as in Example 14, but in this case the centre of the secondary circle occupies a position on the XOY -surface

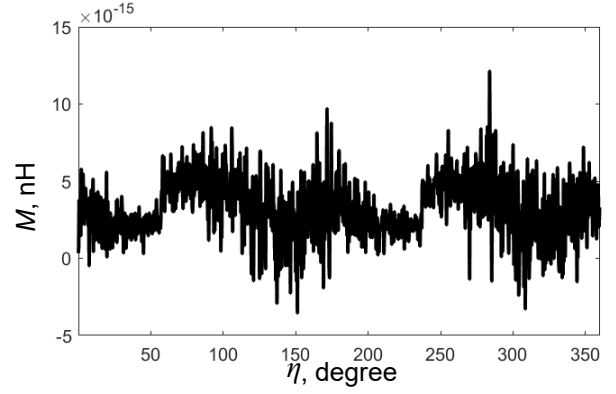


Fig. 14. The chaotic distribution of the absolute error against the η angle in Example 16.

with the following coordinates $x_C = y_C = 10$ cm and $z_C = 0$. Hence, we have

n	BM, (24), nH	MIM, (23), nH
200	-6.23859×10^{-15}	-8.05774×10^{-15}

Then, again let us rotate the η angle in a range $0 < \eta \leq 360^\circ$, the calculation of mutual inductance demonstrates the chaotic distribution of the small error of calculation, which does not exceeded of 15×10^{-15} nH as shown in Fig. 14. The error is continually distributed without interruption of its continuity at $\eta = 90^\circ$ and 270° in comparing with the application of Babic's and Grover's formula (please, see Example 22, in article [12]). Thus, the segmentation method for the calculation of mutual inductance between two circular filaments arbitrarily orientated in the space with respect to each other does not suffer from the singularity case, when two circles are mutually perpendicular.

D. Mutual inductance between circle and a filament of arbitrary shape

Using the proposed methodology based on (23) and (24), the segmentation method is applied to the calculation of the mutual inductance between the primary circle and filaments arbitrary positioning in the space and having different shapes, which can be defined, for instance, by parametric equations of special curves to generate the input set of points (18). In particular, the following curves such as circular and elliptic arcs, ellipse, spiral, helices and conical helices are considered in the proceeding section.

Beginning with the calculation of mutual inductance between the circle and elliptic arc arbitrary positioning in the space, the secondary filament can be defined as a part of ellipse lying on the xy plane. The ellipse is characterized by its semi-major axis A_σ directed along the x -axis and semi-minor B_σ along the y -axis. The parameter ℓ is defined within the finite interval $[\varphi_0, \varphi_1]$ as shown in Fig. 15. The linear misalignment of the arc is defined by coordinates of point C corresponding to the centre of the ellipse, while the angular misalignment can be determined by Euler's angles denoted by α , β and γ . The

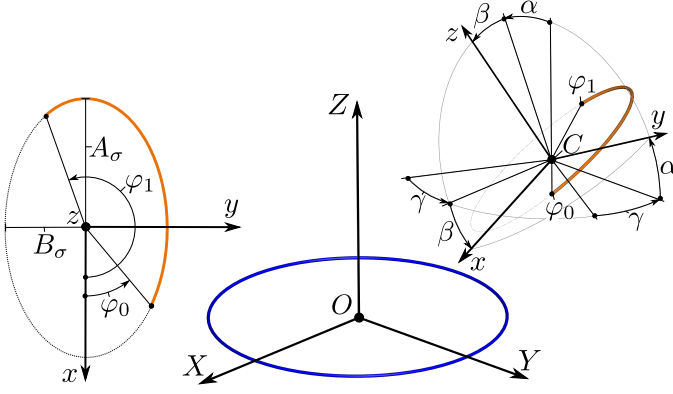


Fig. 15. Elliptic arc on the xy plane is determined as a part of ellipse having the semi-major axis A_σ and semi-minor B_σ within the finite interval $[\varphi_0, \varphi_1]$ (the left side figure); The position of elliptic arc arbitrary orientated in the space with respect to the primary circle (the right side figure).

following relationship between Grover's and Euler's angles is true [12]:

$$\begin{cases} \sin \beta = \sin \eta \sin \theta; \\ \cos \beta \sin \alpha = \cos \eta \sin \theta. \end{cases} \quad (29)$$

According to Fig. 15, the input points can be calculated as follows

$$\underline{p}_i(h_i) = \begin{bmatrix} x_C \\ y_C \\ z_C \end{bmatrix} + \underline{\Delta}_\gamma^T \underline{\Delta}_\alpha^T \underline{\Delta}_\beta^T \begin{bmatrix} A_\sigma \cos h_i \\ B_\sigma \sin h_i \\ 0 \end{bmatrix}, \quad i = 0 \dots n, \quad (30)$$

where

$$\underline{\Delta}_\gamma = \begin{bmatrix} \cos \gamma & \sin \gamma & 0 \\ -\sin \gamma & \cos \gamma & 0 \\ 0 & 0 & 1 \end{bmatrix}, \quad \underline{\Delta}_\alpha = \begin{bmatrix} 1 & 0 & 0 \\ 0 & \cos \alpha & \sin \alpha \\ 0 & -\sin \alpha & \cos \alpha \end{bmatrix} \quad (31)$$

$$\underline{\Delta}_\beta = \begin{bmatrix} \cos \beta & 0 & -\sin \beta \\ 0 & 1 & 0 \\ \sin \beta & 0 & \cos \beta \end{bmatrix}.$$

Example 17: The primary circle has a radius of $R_p = 1$ m, while the elliptic arc is defined by the ellipse having the semi-major axis $A_\sigma = 1$ m and semi-minor one $B_\sigma = 0.5$ m and within the finite interval $[\varphi_0 = 10^\circ, \varphi_1 = 110^\circ]$. The centre of the ellipse is located at $x_C = 10.0$ cm, $y_C = 10.0$ cm, $z_C = 10.0$ cm. The angular misalignment of the secondary filament is defined by $\alpha = 20.0^\circ$, $\beta = 20.0^\circ$, but γ is changed in a range from 0 to 325.0° . The number of line segments of $n = 200$ is taken. The results of calculation are

γ	FastHenry, nH	BM,(24), nH	MIM, (23), nH
0.0°	368.066	368.191	368.191
35.0°	330.527	329.896	329.896
100.0°	243.600	242.784	242.784
180.0°	214.997	214.6251	214.6251
250.0°	288.439	289.2692	289.2692
300.0°	354.949	356.677	356.677
325.0°	373.121	375.319	375.319

It is clear that an elliptic arc can be transformed into the other curves such as a circular one ($A_\sigma = B_\sigma$,

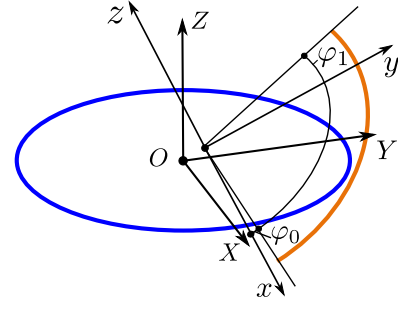


Fig. 16. The scheme for Example 18 (circular arc): $\alpha = 20.0^\circ$, $\beta = 20.0^\circ$ and $\gamma = 0.0^\circ$.

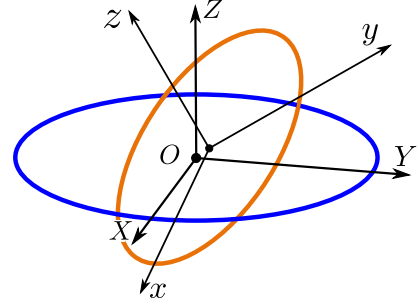


Fig. 17. The scheme for Example 19 (ellipse): $\alpha = 20.0^\circ$, $\beta = 20.0^\circ$ and $\gamma = 0.0^\circ$.

$[\varphi_0 \geq 0, \varphi_1 < 2\pi]$), an ellipse ($A_\sigma \neq B_\sigma$, $[\varphi_0 = 0, \varphi_1 = 2\pi]$) and a circle ($A_\sigma = B_\sigma$, $[\varphi_0 = 0, \varphi_1 = 2\pi]$).

Example 18 (circular arc): The primary circle has a radius of $R_p = 1$ m, while the circular arc is defined by $A_\sigma = B_\sigma = 1$ m within the finite interval $[\varphi_0 = 10^\circ, \varphi_1 = 110^\circ]$. The centre of the secondary circle is located at $x_C = 10.0$ cm, $y_C = 10.0$ cm, $z_C = 10.0$ cm. The angular misalignment of the secondary filament is defined as follows $\alpha = 20.0^\circ$, $\beta = 20.0^\circ$ but γ is changed in a range from 0 to 325.0° as shown in Fig. 16. The number of line segments of $n = 200$ is taken. The results of calculation are

γ	FastHenry, nH	BM, (24), nH	MIM, (23), nH
0.0°	452.190	452.632	452.632
35.0°	463.948	463.5728	463.5728
100.0°	577.401	577.2027	577.2027
180.0°	461.735	461.3058	461.3058
250.0°	522.928	523.709	523.709
300.0°	517.435	519.920	519.920
325.0°	474.681	477.143	477.143

Example 19 (ellipse): The primary circle has a radius of $R_p = 1$ m, while the ellipse is defined by $A_\sigma = 1.0$ m $B_\sigma = 0.5$ m. The centre of the ellipse is located at $x_C = 10.0$ cm, $y_C = 10.0$ cm, $z_C = 10.0$ cm. The angular misalignment of the secondary filament is defined by $\alpha = 20.0^\circ$, $\beta = 20.0^\circ$ and $\gamma = 0.0^\circ$ as shown in Fig. 17. The number of line segments of $n = 200$ is taken. The result of calculation is

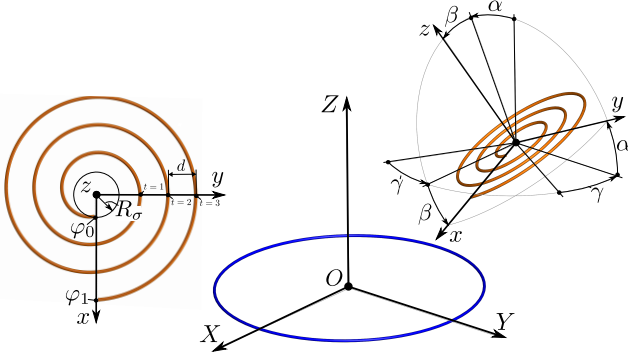


Fig. 18. Spiral on the xy plane is determined by the inner radius of R_σ , the distance between turns d and number of turns t (the left side figure); The position of the spiral arbitrary orientated in the space with respect to the primary circle (the right side figure).

FastHenry, nH	BM, (24), nH	MIM, (23), nH
904.848	905.9695	905.9695

For the case of the calculation of mutual inductance between the circle and a spiral, the secondary filament is lying on the xy plane and its geometry can be characterized by the inner radius R_σ , the number of turns t and the distance between the turns d as shown on Fig. 18. The boundaries of the finite interval of the parameter ℓ are estimated as follows

$$\varphi_0 = 2\pi R_\sigma/d, \varphi_1 = \varphi_0 + 2\pi t. \quad (32)$$

Similar to the elliptic arc, the linear misalignment of the spiral is defined by coordinates of point C , and the angular misalignment is defined by Euler's angles as shown in Fig. 18. The input points are generated by the following equation:

$$\underline{p}_i(h_i) = \begin{bmatrix} x_C \\ y_C \\ z_C \end{bmatrix} + \underline{\Lambda}_\gamma^T \underline{\Lambda}_\alpha^T \underline{\Lambda}_\beta^T \begin{bmatrix} \frac{dh_i}{2\pi} \cos h_i \\ \frac{dh_i}{2\pi} \sin h_i \\ 0 \end{bmatrix}, \quad i = 0 \dots n, \quad (33)$$

where cosine matrices are determined by Eq. (31).

Example 20 (spiral): The primary circle has a radius of $R_p = 0.5$ m. The spiral is defined by the following parameters: the inner radius R_σ is 0.05 m, the distance d is 0.04 m and the number of turns t is 9. The centre C is located at $x_C = 0.6$ m, $y_C = 0.1$ m, and $z_C = 0.7$ m. The angular misalignment is defined as follows $\alpha = 45.0^\circ$, $\beta = -45.0^\circ$, but γ is changed in a range from 0 to 350.0° . The number of line segments n is chosen to be 900 (It is recommended to use at least 100 line segments per turn to have a reasonable accuracy). The results

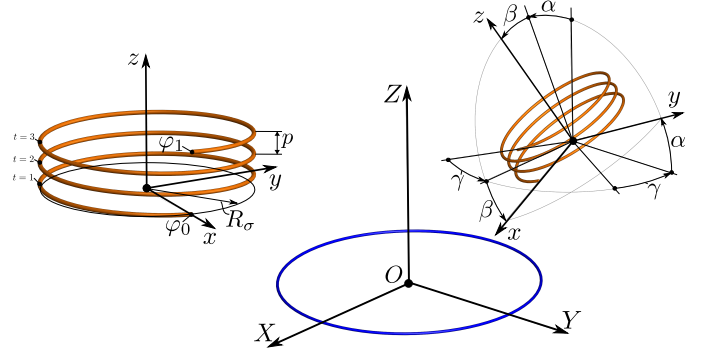


Fig. 19. The helices is determined by its radius R_σ , the pitch p and the number of turns t (the left side figure); The position of the helices arbitrary orientated in the space with respect to the primary circle (the right side figure).

of calculation are

γ	FastHenry, nH	BM, (24), nH	MIM, (23), nH
0.0°	-72.7737	-73.645	-73.645
35.0°	8.58253	8.73071	8.73071
100.0°	179.826	180.625	180.625
180.0°	217.839	217.859	217.859
250.0°	74.2666	73.3870	73.3870
300.0°	-63.6821	-64.2813	-64.2813
350.0°	-86.1984	-87.1184	-87.1184

Further, the calculation of mutual inductance between the circle and a helices is considered. The geometry of helices can be defined on the xyz CF by its radius R_σ , the number of turns t and the pitch p as shown in Fig. 19. The boundaries of the finite interval of the parameter ℓ are

$$\varphi_0 = 0, \varphi_1 = 2\pi t. \quad (34)$$

Similar to previous cases, the linear misalignment of the helices is defined by coordinates of origin C of the xyz CF, and the angular misalignment is defined by Euler's angles as shown in Fig. 19. The following equation can be used to generate the input points:

$$\underline{p}_i(h_i) = \begin{bmatrix} x_C \\ y_C \\ z_C \end{bmatrix} + \underline{\Lambda}_\gamma^T \underline{\Lambda}_\alpha^T \underline{\Lambda}_\beta^T \begin{bmatrix} R_\sigma \cos h_i \\ -R_\sigma \sin h_i \\ \frac{ph_i}{2\pi} \end{bmatrix}, \quad i = 0 \dots n. \quad (35)$$

Example 21 (helices): The primary circle has radius of $R_p = 0.9$ m. The helices is defined by the following parameters: the radius R_σ is 0.6 m, the pitch p is 0.05 m and the number of turns t is 4. The origin C is located at $x_C = 0.3$ m, $y_C = 0.2$ m, $z_C = 0.5$ m. The angular misalignment is characterized by $\alpha = 54.7356^\circ$, $\beta = 0.0^\circ$ and γ is taken from a range from 0 to 335.0° . The number of line segments n is

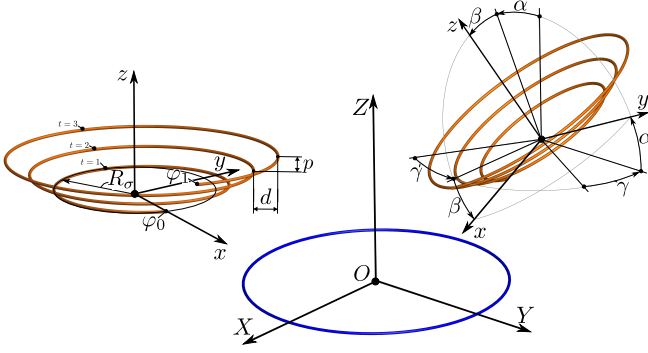


Fig. 20. The conical helices is determined by its radius R_σ , the pitch p , the number of turns t and the distance between the turns d (the left side figure); The position of the conical helices arbitrary orientated in the space with respect to the primary circle (the right side figure).

chosen to be 400. The results of calculation are

γ	FastHenry, nH	BM, (24), nH	MIM, (23), nH
0.0°	-963.374	-965.106	-965.106
35.0°	-1242.69	-1245.91	-1245.91
135.0°	-1892.12	-1893.43	-1893.43
180.0°	-1537.51	-1537.38	-1537.38
235.0°	-1025.08	-1024.81	-1024.81
300.0°	-771.485	-771.878	-771.878
335.0°	-835.499	-836.041	-836.041

Finally, the calculation of mutual inductance between the circle and a conical helices is carried out. The geometry of helices can be defined on the xyz CF by its radius R_σ , the number of turns t , the pitch p and the distance between turns d as shown in Fig. 20. The boundaries of the finite interval of the parameter ℓ are

$$\varphi_0 = 2\pi R_\sigma/d, \varphi_1 = \varphi_0 + 2\pi t. \quad (36)$$

The linear misalignment of the conical helices is defined by coordinates of origin C of the xyz CF, and the angular misalignment is defined by Euler's angles as shown in Fig. 20. The following equation generates the input points:

$$\underline{p}_i(h_i) = \begin{bmatrix} x_C \\ y_C \\ z_C \end{bmatrix} + \underline{\Delta}_\gamma^T \underline{\Delta}_\alpha^T \underline{\Delta}_\beta^T \begin{bmatrix} R_\sigma h_i \cos h_i \\ -R_\sigma h_i \sin h_i \\ \frac{p(h_i - \varphi_0)}{2\pi} \end{bmatrix}, \quad i = 0 \dots n. \quad (37)$$

Example 22 (conical helices): The primary circle has radius of $R_p = 0.9$ m. The conical helices is defined by the following parameters: the radius R_σ is 0.0 m, the pitch p is 0.1 m, the number of turns t is 4 and the distance d is 0.04 m. The origin C is located at $x_C = 0.3$ m, $y_C = 0.2$ m, $z_C = 0.5$ m. The angular misalignment is characterized by $\alpha = 135^\circ$, $\beta = 0.0^\circ$ and γ is taken from 0 to 335.0° as shown in Fig. 21. The number of line segments n is chosen to be 400. The results of calculation are

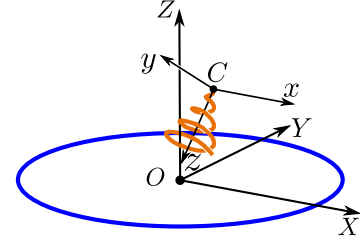


Fig. 21. The scheme for Example 22 (conical helices): $\alpha = 135.0^\circ$, $\beta = 0.0^\circ$ and $\gamma = 0.0^\circ$.

γ	FastHenry, nH	BM, (24), nH	MIM, (23), nH
0.0°	27.2802	27.2225	27.2225
35.0°	29.1615	28.8732	28.8732
135.0°	68.2821	68.401	68.401
180.0°	84.7305	85.15068	85.15068
235.0°	79.8669	79.6694	79.6694
300.0°	47.0447	46.7936	46.7936
335.0°	32.3496	32.1987	32.1987

V. CONCLUSION

In this article, two novel formulas for calculation of mutual inductance between a circular filament and line segment arbitrarily positioning in the space were derived by means of mutual inductance method and Babić's method, respectively. These two formulas were expressed via the integral relationships, whose kernels include the elliptic functions of the first and second kinds. The two formulas are successfully validated to each other mutually and numerically via the *FastHenry* software.

Using the fact that any curve can be interpolated with a desired accuracy by a finite number of line segments, a segmentation method for calculation of the mutual inductance between the primary circle and a filament having an arbitrary shape is proposed and successfully developed based on the two derived formulas. It is shown that for calculation of mutual inductance between the primary circle and the secondary filament of an arbitrarily shape by means of segmentation method based on (23) and (24), the set of points belonging to the secondary filament as the input data is only needed.

The proposed segmentation method is successfully applied to the calculation of the mutual inductance between the primary circle and filaments arbitrary positioning in the space and having different shapes such as circular and elliptic arcs, ellipse, spiral, helices and conical helices. All results of calculation are in a good agreement with the reference examples and successfully validated by the *FastHenry* software.

Considering a limit case, when the radius of the primary circle is trending to zero, the developed methodology can be used for calculation of the magnetic flux density and its gradient generated by a current-carrying arbitrarily shaped filament. As a result, the force and stiffness between two arbitrarily shaped current-carrying filaments can be calculated by using

developed methodology. This matter can be considered as our future work.

ACKNOWLEDGMENT

S.S.K., E.R.M., and K.V.P. acknowledge with thanks the support from German Research Foundation (Grant KO 1883/37-1) under the priority programme SPP 2206.

REFERENCES

- [1] E. B. Rosa, *The self and mutual inductances of linear conductors*. US Department of Commerce and Labor, Bureau of Standards, 1908.
- [2] F. W. Grover, *Inductance calculations : working formulas and tables*, special ed. prepared for instrument society of america ed. Research Triangle Park, N.C. : Instrument Society of America, 1981, reprint. Originally published: New York : Van Nostrand, 1946. With publisher's comment.
- [3] H. B. Dwight, *Electrical Coils and Conductors: Their Electrical Characteristics*. McGraw-Hill, 1945.
- [4] C. Snow, *Formulas for computing capacitance and inductance*. US Govt. Print. Off., 1954, vol. 544.
- [5] L. A. Zeitlin, *Induktivnosti provodov i konturov (Inductances of wires and loops)*. Leningrad - Moskva: Gosenergoizdat, 1950.
- [6] P. L. Kalantarov and L. A. Zeitlin, *Raschet induktivnostey (Calculation of Inductances)*, 3rd ed. Leningrad: Energoatomizdat, 1986.
- [7] E. Okress, D. Wroughton, G. Comenetz, P. Brace, and J. Kelly, "Electromagnetic levitation of solid and molten metals," *Journal of Applied Physics*, vol. 23, no. 5, pp. 545–552, 1952.
- [8] B. K. Narukullapati and T. K. Bhattacharya, "Determination of a stable lateral region of a floating disc—Mathematical analysis and FEM simulation," *Alexandria Engineering Journal*, vol. 60, no. 3, pp. 3107–3118, 2021.
- [9] E. Paredes, G. B. Galán, J. A. Veira, J. Mosqueira, L. Romaní, and G. Domarco, "Measurements of the currents induced in coaxially confronted superconducting rings," *Engineering Research Express*, vol. 3, no. 1, p. 015010, 2021.
- [10] R. Ravaut, G. Lemarquand, V. Lemarquand, S. Babic, and C. Akyel, "Mutual inductance and force exerted between thick coils," *Progress In Electromagnetics Research*, vol. 102, pp. 367–380, 2010.
- [11] S. Babic, F. Sirois, C. Akyel, and C. Girardi, "Mutual inductance calculation between circular filaments arbitrarily positioned in space: Alternative to Grover's formula," *IEEE Transactions on Magnetics*, vol. 46, no. 9, pp. 3591–3600, Sept 2010. [Online]. Available: <https://doi.org/10.1109/TMAG.2010.2047651>
- [12] K. V. Poletkin and J. G. Korvink, "Efficient calculation of the mutual inductance of arbitrarily oriented circular filaments via a generalisation of the Kalantarov-Zeitlin method," *Journal of Magnetism and Magnetic Materials*, vol. 483, pp. 10–20, 2019. [Online]. Available: <https://www.sciencedirect.com/science/article/pii/S0304885318337703>
- [13] D. Wu, F. Cheng, and C. Huang, "Analytical computation of mutual inductance between two rectangular spiral coils with misalignments for wireless power applications," *Microwave and Optical Technology Letters*, vol. 62, no. 2, pp. 637–642, 2020. [Online]. Available: <https://onlinelibrary.wiley.com/doi/abs/10.1002/mop.32074>
- [14] J. Yi, P. Yang, Z. Li, P. Kong, and J. Li, "Mutual Inductance Calculation of Circular Coils for an Arbitrary Position with a Finite Magnetic Core in Wireless Power Transfer Systems," pp. 1–1. [Online]. Available: <https://ieeexplore.ieee.org/document/9826855>
- [15] N. Pirinççi and H. Altun, "A new analytical study on mutual inductance calculations for wireless power transfer using magnetic vector potential," *IEEE Trans. Magn.*, vol. 58, no. 8, pp. 1–14, 2022. [Online]. Available: <https://ieeexplore.ieee.org/document/9796599>
- [16] S. I. Babic and C. Akyel, "Magnetic force calculation between thin coaxial circular coils in air," *IEEE Transactions on Magnetics*, vol. 44, no. 4, pp. 445–452, 2008.
- [17] —, "Torque calculation between circular coils with inclined axes in air," *International Journal of Numerical Modelling: Electronic Networks, Devices and Fields*, vol. 24, no. 3, pp. 230–243, 2011.
- [18] S. I. Babic, C. Akyel, Y. Ren, and W. Chen, "Magnetic force calculation between circular coils of rectangular cross section with parallel axes for superconducting magnet," *Progress In Electromagnetics Research*, vol. 37, pp. 275–288, 2012. [Online]. Available: <http://dx.doi.org/10.2528/PIERB11110508>
- [19] S. Babic, "Vector potential, magnetic field, mutual inductance, magnetic force, torque and stiffness calculation between current-carrying arc segments with inclined axes in air," *Physics*, vol. 3, no. 4, pp. 1054–1087, 2021. [Online]. Available: <https://www.mdpi.com/2624-8174/3/4/67>
- [20] K. V. Poletkin, "Calculation of magnetic force and torque between two arbitrarily oriented circular filaments using Kalantarov-Zeitlin's method," *Int J Mech Sci*, vol. 220, p. 107159, 2022.
- [21] R. Ravaut, G. Lemarquand, S. Babic, V. Lemarquand, and C. Akyel, "Cylindrical magnets and coils: Fields, forces, and inductances," *IEEE Trans. Magn.*, vol. 46, no. 9, pp. 3585–3590, 2010.
- [22] K. Poletkin and S. Babic, "Magnetic stiffness calculation for the corresponding force between two current-carrying circular filaments arbitrarily oriented in the space," p. accepted for publication.
- [23] U.-M. Jow and M. Ghovanloo, "Design and optimization of printed spiral coils for efficient transcutaneous inductive power transmission," *IEEE Transactions on biomedical circuits and systems*, vol. 1, no. 3, pp. 193–202, 2007.
- [24] Y. P. Su, X. Liu, and S. Y. R. Hui, "Mutual inductance calculation of movable planar coils on parallel surfaces," *IEEE Transactions on Power Electronics*, vol. 24, no. 4, pp. 1115–1123, April 2009.
- [25] S. Y. Chu and A. T. Avestruz, "Transfer-power measurement: A non-contact method for fair and accurate metering of wireless power transfer in electric vehicles," in *2017 IEEE 18th Workshop on Control and Modeling for Power Electronics (COMPEL)*, July 2017, pp. 1–8.
- [26] A. Shiri and A. Shoulaie, "A new methodology for magnetic force calculations between planar spiral coils," *Progress In Electromagnetics Research*, vol. 95, pp. 39–57, 2009.
- [27] R. Ravaut, G. Lemarquand, and V. Lemarquand, "Force and stiffness of passive magnetic bearings using permanent magnets, part 1: Axial magnetization," *IEEE Trans. Magn.*, vol. 45, no. 7, p. 2996, 2009.
- [28] S. Obata, "A muscle motion solenoid actuator," *Electrical Engineering in Japan*, vol. 184, no. 2, pp. 10–19, 2013.
- [29] K. Poletkin, A. Chernomorsky, C. Shearwood, and U. Wallrabe, "A qualitative analysis of designs of micromachined electromagnetic inductive contactless suspension," *International Journal of Mechanical Sciences*, vol. 82, pp. 110–121, May 2014. [Online]. Available: <http://authors.elsevier.com/sd/article/S0020740314000897>
- [30] Z. Lu, K. Poletkin, B. den Hartogh, U. Wallrabe, and V. Badilita, "3D micro-machined inductive contactless suspension: Testing and modeling," *Sensors and Actuators A Physical*, vol. 220, pp. 134–143, 2014. [Online]. Available: <http://dx.doi.org/10.1016/j.sna.2014.09.017>
- [31] K. Poletkin, Z. Lu, U. Wallrabe, J. Korvink, and V. Badilita, "Stable dynamics of micro-machined inductive contactless suspensions," *Int J Mech Sci*, vol. 131–132, pp. 753 – 766, 2017. [Online]. Available: <http://www.sciencedirect.com/science/article/pii/S0020740316306555>
- [32] K. V. Poletkin, A. I. Chernomorsky, and C. Shearwood, "A proposal for micromachined accelerometer, base on a contactless suspension with zero spring constant," *IEEE Sensors J.*, vol. 12, no. 07, pp. 2407–2413, 2012.
- [33] K. V. Poletkin and J. G. Korvink, "Modeling a pull-in instability in micro-machined hybrid contactless suspension," vol. 7, no. 1, p. 11, 2018.
- [34] K. Poletkin, "Static pull-in behavior of hybrid levitation micro-actuators: simulation, modelling and experimental study," *IEEE/ASME Transactions on Mechatronics*, pp. 753–764, 2020. [Online]. Available: <https://doi.org/10.1109/TMECH.2020.2999516>
- [35] —, "On the static pull-in of tilting actuation in electromagnetically levitating hybrid micro-actuator: Theory and experiment," *Actuators*, vol. 10, no. 10, 2021. [Online]. Available: <https://www.mdpi.com/2076-0825/10/10/256>
- [36] T. Theodoulidis and R. J. Ditchburn, "Mutual impedance of cylindrical coils at an arbitrary position and orientation above a planar conductor," *IEEE Transactions on Magnetics*, vol. 43, no. 8, pp. 3368–3370, Aug 2007.
- [37] M. Sawan, S. Hashemi, M. Sehil, F. Awwad, M. Hajj-Hassan, and A. Khoulas, "Multicoils-based inductive links dedicated to power up implantable medical devices: modeling, design and experimental results," *Biomedical Microdevices*, vol. 11, no. 5, p. 1059, Jun 2009. [Online]. Available: <https://doi.org/10.1007/s10544-009-9323-7>
- [38] S. Kuznetsov and J. K. Guest, "Topology optimization of magnetic source distributions for diamagnetic and superconducting levitation," *Journal of Magnetism and Magnetic Materials*, vol. 438, pp. 60 – 69, 2017. [Online]. Available: <http://www.sciencedirect.com/science/article/pii/S0304885316319515>
- [39] D. Hoult and B. Tomanek, "Use of mutually inductive coupling in probe design," *Concepts in Magnetic Resonance*, vol. 15, no. 4, pp.

- 262–285, 2002. [Online]. Available: <https://onlinelibrary.wiley.com/doi/abs/10.1002/cmr.10047>
- [40] N. Spengler, P. T. While, M. V. Meissner, U. Wallrabe, and J. G. Korvink, “Magnetic lenz lenses improve the limit-of-detection in nuclear magnetic resonance,” *PLOS ONE*, vol. 12, no. 8, pp. 1–17, 08 2017. [Online]. Available: <https://doi.org/10.1371/journal.pone.0182779>
 - [41] G. D. Angelis, V. Pasku, A. D. Angelis, M. Dionigi, M. Mongiardo, A. Moschitta, and P. Carbone, “An indoor ac magnetic positioning system,” *IEEE Transactions on Instrumentation and Measurement*, vol. 64, no. 5, pp. 1267–1275, May 2015.
 - [42] F. Wu, J. Jeon, S. K. Moon, H. J. Choi, and H. Son, “Voice coil navigation sensor for flexible silicone intubation,” *IEEE/ASME Transactions on Mechatronics*, vol. 21, no. 2, pp. 851–859, April 2016.
 - [43] X. Zhang, C. Quan, and Z. Li, “Mutual inductance calculation of circular coils for an arbitrary position with electromagnetic shielding in wireless power transfer systems,” *IEEE Transactions on Transportation Electrification*, pp. 1–1, 2021.
 - [44] S. Y. Chu, X. Cui, X. Zan, and A.-T. Avestruz, “Transfer-power measurement using a non-contact method for fair and accurate metering of wireless power transfer in electric vehicles,” *IEEE Transactions on Power Electronics*, vol. 37, no. 2, pp. 1244–1271, 2021.
 - [45] B. Gulbahar, “A communication theoretical analysis of multiple-access channel capacity in magneto-inductive wireless networks,” *IEEE Transactions on Communications*, vol. 65, no. 6, pp. 2594–2607, June 2017.
 - [46] M. Kamon, M. J. Tsuk, and J. K. White, “Fasthenry: a multipole-accelerated 3-D inductance extraction program,” *IEEE Transactions on Microwave Theory and Techniques*, vol. 42, no. 9, pp. 1750–1758, Sept 1994.